



ELSEVIER

Contents lists available at ScienceDirect

## Comptes Rendus Mecanique

www.sciencedirect.com



Separation flow control

## Fluidic control of wake-flow behind a two-dimensional square back bluff body

*Contrôle du sillage d'un corps bidimensionnel à culot droit*Sébastien Chaligné<sup>a,b</sup>, Thomas Castelain<sup>a,c,\*</sup>, Marc Michard<sup>a</sup>,  
Damien Chacaton<sup>b</sup>, Daniel Juvé<sup>a</sup><sup>a</sup> LMFA, École centrale de Lyon, 36, avenue Guy-de-Collongue, 69134 Écully cedex, France<sup>b</sup> Volvo Group Truck Technology, Cab Engineering Lyon, 99, route de Lyon, 69806 Saint-Priest cedex, France<sup>c</sup> Université Lyon-1, boulevard du 11-Novembre-1918, 69622 Villeurbanne cedex, France

## ARTICLE INFO

## Article history:

Received 4 September 2013

Accepted 14 December 2013

Available online 5 June 2014

## Keywords:

Flow control

Synthetic jet

Square-back

## Mots-clés:

Contrôle d'écoulement

Jet synthétique

Culot droit

## ABSTRACT

This experimental study deals with wake-flow fluidic control behind a two-dimensional square back geometry positioned close to the ground. The fluidic control system is made of pulsed jets positioned at the upper edge of the model base. The objective of the fluidic action is to modify the wake-flow development, and as a consequence the static pressure distribution over the model base and hence the pressure drag. The main concern of this study is to determine to what extent the presence of a flow confined between the model and the floor influences the effectiveness of the control. Static pressure measurements at the model base and wake-flow characteristics derived from PIV measurements at a high acquisition frequency indicate global similarities between a case where an underbody flow exists and a case where this underbody flow is absent. For low actuation frequencies, discrepancies in the way the coherent structures due to the control develop in the shear layer appear.

© 2014 Académie des sciences. Published by Elsevier Masson SAS. All rights reserved.

## R É S U M É

Une méthode de contrôle d'écoulement en boucle ouverte est appliquée à un écoulement de sillage d'une maquette bidimensionnelle à culot droit. Un système de jets pulsés soufflant à l'arrêt du culot de la maquette est utilisé. L'objectif de l'action fluidique est de modifier le développement de l'écoulement de sillage et par conséquent la répartition de pression statique au culot de la maquette, donc la traînée de pression. Une attention particulière est portée dans cette étude à l'influence d'un écoulement de soubassement entre la maquette et le sol de la veine d'essais sur la pertinence du contrôle. Des mesures de pression statique au culot et les caractéristiques principales de l'écoulement à l'aval de la maquette, obtenues par l'analyse de mesures PIV à haute fréquence d'acquisition, indiquent des similitudes entre un cas où un écoulement de soubassement existe et un cas sans écoulement de soubassement. Pour les plus faibles fréquences d'actionnement

\* Corresponding author at: LMFA, UMR CNRS 5509, École centrale de Lyon, 36, avenue Guy-de-Collongue, 69134 Écully cedex, France.

E-mail address: [thomas.castelain@ec-lyon.fr](mailto:thomas.castelain@ec-lyon.fr) (T. Castelain).

testées, on observe des spécificités propres à chaque cas dans la manière dont les structures cohérentes induites par le contrôle se développent dans la couche de cisaillement.

© 2014 Académie des sciences. Published by Elsevier Masson SAS. All rights reserved.

## 1. Introduction

Fluidic control has been experimentally tested on a two-dimensional square back geometry of height  $H$  positioned at a distance  $G$  from the ground.

The case where the ground clearance  $G$  is not null, in other words where an underbody flow develops, is of primary interest in ground vehicles aerodynamics. The aim of this study is to shed some light on the differences in the results obtained for two different configurations. The first one corresponds to a zero underbody flow condition ( $G/H = 0$ ), thus a backward-facing step for which flow control have been previously implemented for instance in channel flows [1]. The second configuration corresponds to a ratio  $G/H$  non-null but still small. This configuration will be considered here as a reference configuration and will thus be analyzed more in details than the other one. The motivation to set  $G/H$  to a small value is twofold. It is well known that the vortex shedding present in the wake of two-dimensional blunt bodies placed in free stream no longer exists if a flat surface is sufficiently close to the body [2,3]. Also the mean drag is known to be significantly higher when a vortex shedding occurs [4]. Thus a sufficiently small value of  $G/H$  prevents vortex shedding and allows the comparative study with a backward-facing step-like flow. Furthermore, this geometrical characteristic can be found for example on the long-haul truck trailers where the ratio  $G/H$  ranges from 0.3 down to very low values, depending on the trailer type.

## 2. Experimental setup

Experiments are conducted in an open test section wind tunnel. The flow comes out of a nozzle with an exit square section of  $500 \times 500 \text{ mm}^2$ . The free stream velocity  $U_\infty$  is set to  $25 \text{ m}\cdot\text{s}^{-1}$  and constantly monitored by using a Pitot tube. The model used is a two-dimensional bluff body represented in Fig. 1. This model is positioned at a distance of 300 mm from the nozzle. Its length  $L$ , height  $H$  and width  $W$  are respectively 555 mm, 100 mm and 380 mm, resulting in a Reynolds number  $Re_H$  of 176000. Two configurations are reported here, depending on the associated value of the ground clearance ratio  $G/H$ . The first one corresponds to  $G/H = 0$ , and the second one to  $G/H = 0.04$ . In the latter configuration, the underbody flow velocity  $U_u$  has been measured to 0.6 times the free stream velocity. Two lateral transparent plates are positioned on each side of the model to ensure two-dimensional statistical flow properties in the central part of the geometry, where pressure and velocity measurements are performed. These properties are confirmed in the central upper part of the model by comparing the velocity profiles at different locations in the  $Y$  direction, 5 mm upstream the rear edge. The velocity profiles compare well over at least 60% of the model width, the reference profile being that measured in the median plane.

The description of the control system is given in details in [5]. In brief, a pulsed jet system consisting of seven rapid solenoid valves placed upstream of circular-to-rectangular nozzles is used here. Each nozzle exit section corresponds to a rectangular slot of 0.3-mm thickness and 50-mm spanwise length. Slots are positioned at the upper rear edge of the model and are oriented so that the jet angle with respect to the free stream flow direction is equal to  $45^\circ$ , as illustrated in Fig. 1. The solenoid valves are driven in open loop and in phase with an actuation frequency  $F_{ac}$  and a duty cycle of 50%. The

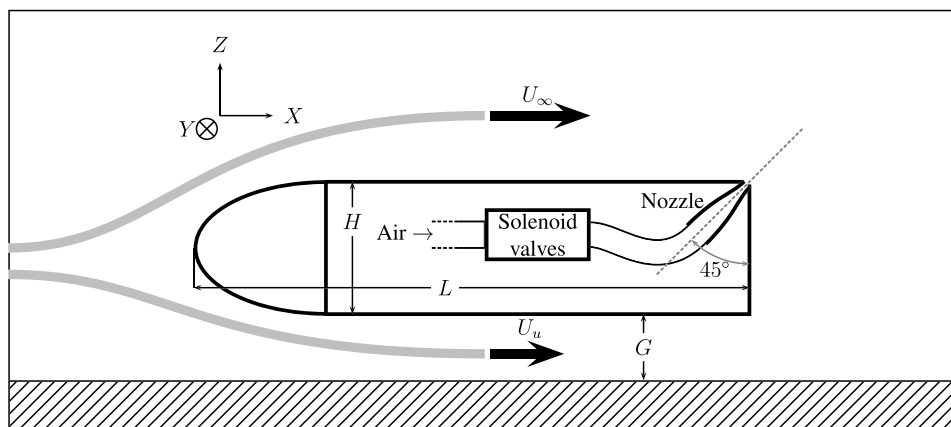
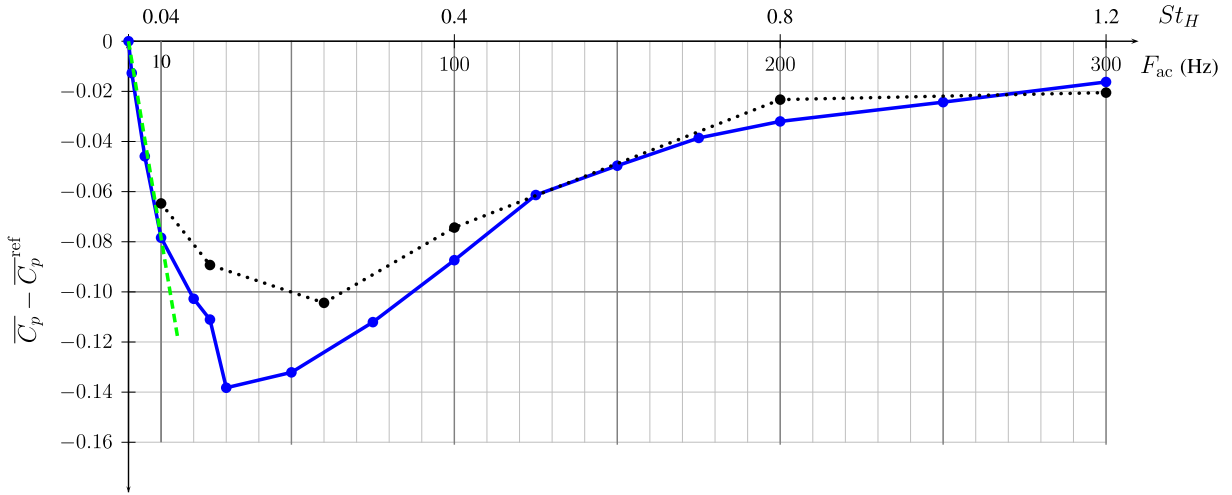


Fig. 1. Side view of the two-dimensional model with pulsed jet system. The normal to the plane of symmetry is the  $Y$  axis.

**Table 1**  
Reference mean pressure coefficients  $\overline{C_p}^{\text{ref}}$  at the model base, without control, for the two different configurations.

	$G/H = 0$	$G/H = 0.04$
$\overline{C_p}^{\text{ref}}$	-0.122	-0.180



**Fig. 2.** (Color online.) Mean static pressure coefficient  $\overline{C_p}$  measured at the base of the model function of the actuation frequency  $F_{ac}$ . The values of the pressure coefficient are relative to the reference value  $\overline{C_p}^{\text{ref}}$  obtained without control (for  $F_{ac} = 0$ , the pulsed jet system is off). (■ ■ ■ ■)  $G/H = 0$ ; (—●—)  $G/H = 0.04$ ; (—■—) linear fit for the low-frequency actuation.

relative pressure upstream the valves is set to 1 bar. Wall pressure measurements are carried out at the base of the model. Fifteen wall pressure taps are distributed along the median plane, each being connected to a Scanivalve system coupled with a Furness 0–200-mm H<sub>2</sub>O manometer. Time-averaged values over two seconds are collected and the spatial average of these values provides an estimate of the mean pressure  $\overline{p}$  at the model base. The results are provided here in terms of mean pressure coefficient  $\overline{C_p}$ , defined in (1) by use of the air density  $\rho$  and the free stream static pressure  $p_0$ :

$$\overline{C_p} = \frac{\overline{p} - p_0}{1/2 \rho U_\infty^2} \tag{1}$$

Particle Image Velocimetry measurements are performed in the near-wake median plane. The PIV set-up and the processing details are described in [5]. In brief, sets of 2500 image couples are recorded at a rate of 3125 Hz. The dimensions of the field of view are  $L_x/H = 2.15$  horizontally and  $L_z/H = 1.34$  vertically.

### 3. Results

The analysis of the mean pressure and flow-field characteristics is given first for the cases without control. On this basis, the results for controlled configurations are further discussed.

#### 3.1. Mean pressure coefficient at the model base

The measured values of the mean pressure coefficient at the model base without control are reported in Table 1. These values are used in the following as reference values, and are therefore noted  $\overline{C_p}^{\text{ref}}$ . The mean pressure coefficient in the  $G/H = 0.04$  case is, in absolute value, about 50% higher than that of the  $G/H = 0$  case. This result is consistent with the monotonic decrease of  $\overline{C_p}$  with  $G/H$  obtained in previous experimental studies [6,7]. The mean pressure coefficient values obtained with control are presented in Fig. 2 for the two values of ground clearance considered here. In each case on this figure, the corresponding reference value  $\overline{C_p}^{\text{ref}}$  obtained with the pulsed jet system off is subtracted to the actual mean pressure coefficient value. In each case also, the evolution of  $\overline{C_p}$  with the actuation frequency presents a minimum value for an actuation frequency around 50 Hz, the precise value of the actuation frequency depending on the configuration; for higher actuation frequencies, the mean pressure coefficient keeps increasing and seems to reach an asymptotic value below  $\overline{C_p}^{\text{ref}}$ . Thus, the control only decreases the base pressure with respect to the reference case, and as a consequence increases the pressure drag. The similarity in the evolution of  $\overline{C_p}$  between the two configurations contrasts with the very different values of  $\overline{C_p}^{\text{ref}}$  commented above. The fact that for given actuation frequencies, a doubling in the  $\overline{C_p}$  values with

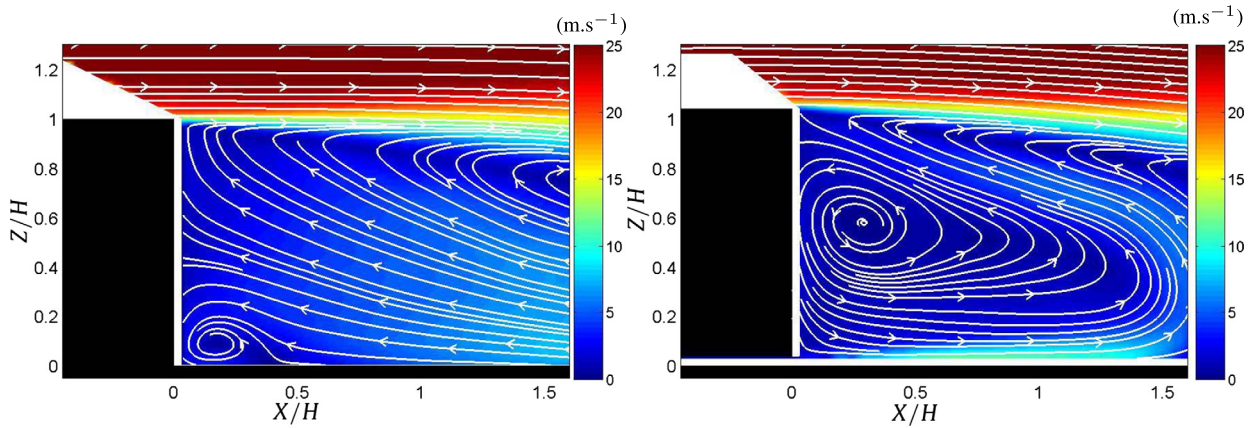


**Fig. 3.** (Color online.) Norm of mean velocity  $\bar{u}$ , without control, for (a)  $G/H = 0$ , (b)  $G/H = 0.04$ . The streamlines superimposed on the colormap are given to highlight the local flow direction.

respect to  $\bar{C}_p^{\text{ref}}$  is obtained, is linked to changes in the wake flow characteristics, as will be described in Section 3.2. Moreover, the presence of a minimum in the evolution of  $\bar{C}_p$  with the actuation frequency suggests that different control-induced flow phenomena contribute to a diminution of  $\bar{C}_p$ . Finally, one may note that, for the  $G/H = 0.04$  configuration, the evolution of  $\bar{C}_p$  with the actuation frequency, for the low-frequency values up to  $F_{\text{ac}} = 10$  Hz, exhibits a linear behavior. It is supposed that this property also applies to the  $G/H = 0$  configuration, even if the lack of data in the low-frequency region for this configuration does not permit to prove this assumption. This linear behavior is further interpreted on the basis of the wake flow characteristics.

### 3.2. Near wake-flow development

The analysis of the velocity flow-field is performed by use of statistical approaches. For the reference flows, the classical Reynolds decomposition allows to separate in any quantity  $q(\mathbf{x}, t)$  the time-average value  $\bar{q}(\mathbf{x})$  from the fluctuating part  $q'$ , using Eq. (2). In controlled cases moreover, where the actuation cycles provide a periodic time basis, the triple decomposition is also used to separate in the fluctuating part of  $q$ , the contribution of periodic perturbations  $\tilde{q}$  at the actuation frequency from the stochastic fluctuations  $q''$ , as illustrated in Eq. (3). The phase average  $\langle q \rangle$  of the quantity  $q$  is also defined in Eq. (3), noting  $\tau$  as the time delay within the period of one actuation cycle.

$$q(\mathbf{x}, t) = \bar{q}(\mathbf{x}) + q'(\mathbf{x}, t) \quad (2)$$

$$q(\mathbf{x}, t) = \bar{q}(\mathbf{x}) + \tilde{q}(\mathbf{x}, \tau) + q''(\mathbf{x}, t) = \langle q \rangle(\mathbf{x}, \tau) + q''(\mathbf{x}, t) \quad (3)$$

#### 3.2.1. Mean-flow characteristics without control

Velocity maps given in Fig. 3 clearly highlight the fundamental differences in the wake flow between the two configurations considered. For  $G/H = 0$ , the wake region close to the ground is dominated by the recirculating flow coming from the region downstream the field of view; a small counter-clockwise rotating recirculation is located next to the bottom corner of the model. For  $G/H = 0.04$ , the underbody flow is responsible for a recirculation located at mid-height in the wake of the model and much larger than that observed in the  $G/H = 0$  case. These features are thought to induce the differences in  $\bar{C}_p^{\text{ref}}$  values presented in Section 3.1. In the other hand, the shear layer development is not significantly affected by the presence of the underbody flow in the  $G/H = 0.04$  case, over the  $X/H$  range considered here. To illustrate quantitatively this property, an estimate of the momentum thickness  $\delta_\theta$  is computed by considering, for each longitudinal location  $X$ , the vertical profile above the point where the longitudinal velocity is zero. The evolution of  $\delta_\theta$  with  $X/H$ , presented in Fig. 4, compares well between the two cases. This being said, the  $\delta_\theta$  values are larger for the  $G/H = 0$  case than for the  $G/H = 0.04$  case; this is attributed to an installation effect consisting in a change in the boundary layer thickness over the model and is therefore not characteristic of any underbody flow effect.

#### 3.2.2. Mean-flow characteristics with control

The effects of the control are illustrated here on the mean flow characteristics. Of particular interest are the actuation frequencies  $F_{\text{ac}} = 10$  Hz and 100 Hz, which provide, for a given ground clearance, nearly the same diminution in the mean pressure coefficient, as indicated in Fig. 2. In Fig. 5 the corresponding velocity maps for  $G/H = 0$  and 0.04 are presented. A recirculation region is visible in the mean wake-flow. The control has a noticeable effect on the location of the recirculation centers, that additionally depends on the ground clearance value. Indeed, one may notice that the recirculation center in the  $G/H = 0$  case is considerably moved downstream when the actuation frequency varies from 10 to 100 Hz

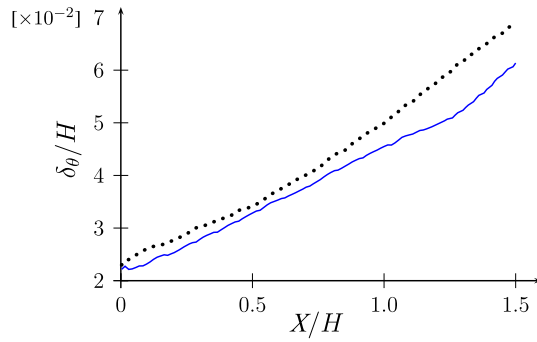


Fig. 4. (Color online.) Evolution of  $\delta_\theta$  with  $X/H$ . (•••••)  $G/H = 0$ ; (—)  $G/H = 0.04$ .

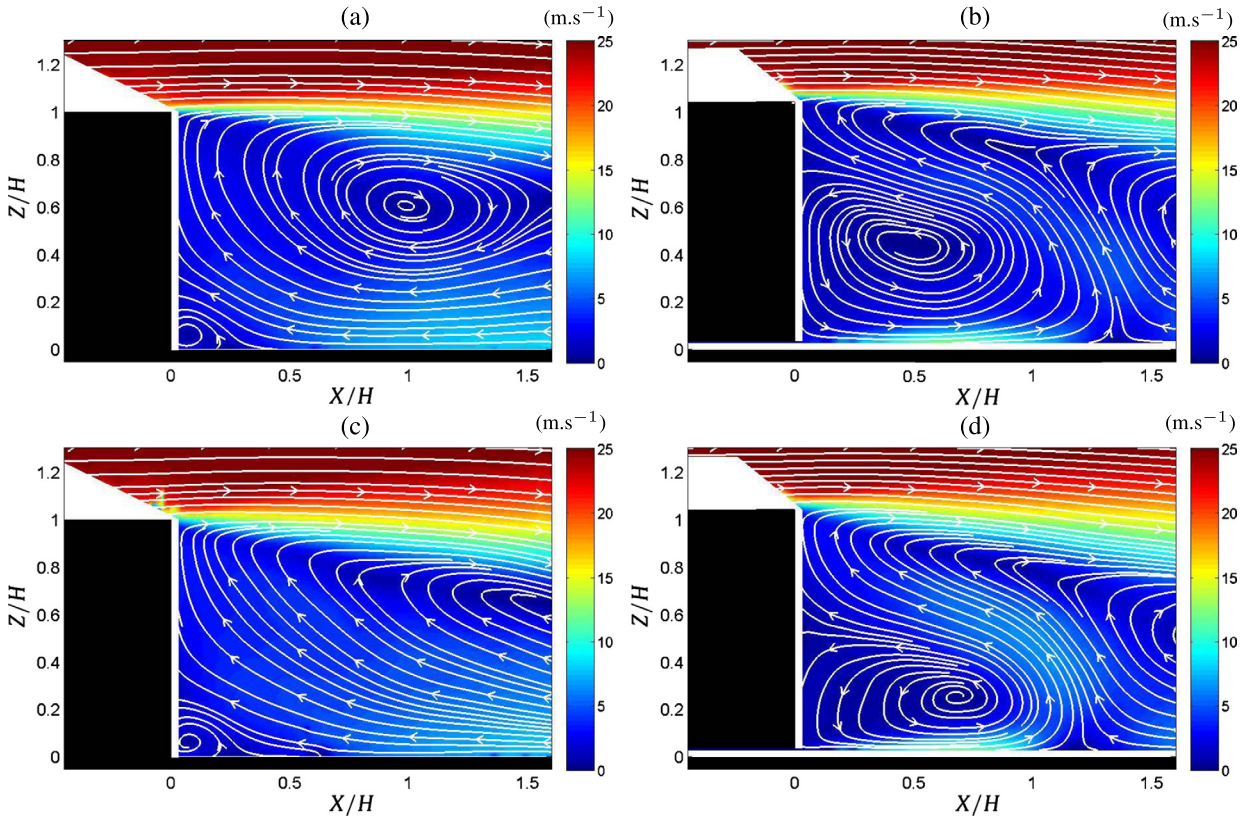
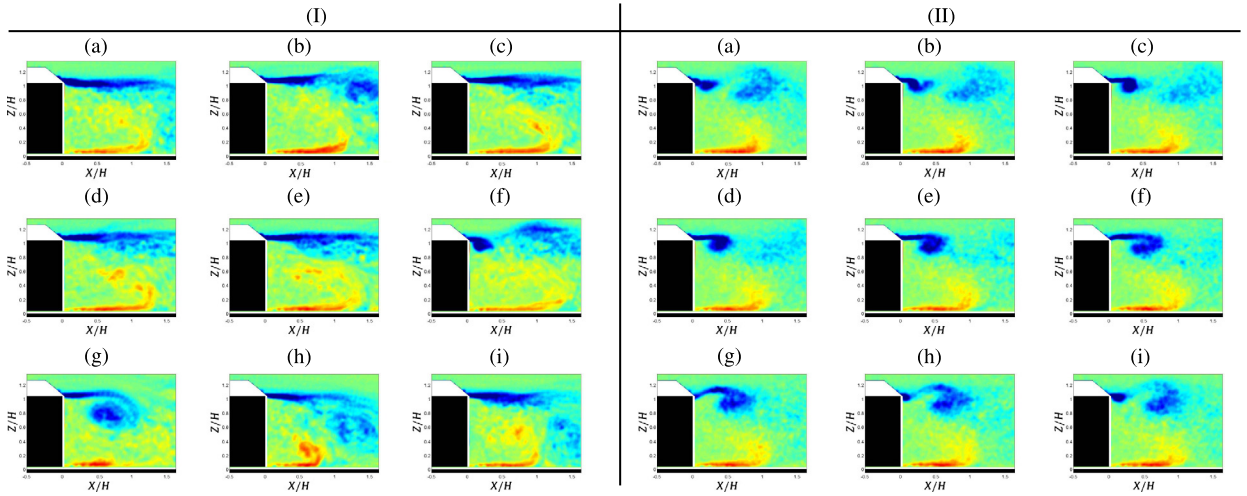


Fig. 5. (Color online.) Norm of mean velocity  $\bar{u}$ , with control, for (a,c)  $G/H = 0$ , (b,d)  $G/H = 0.04$  and controlled jets actuated at (a,b)  $F_{ac} = 10$  Hz and (c,d)  $F_{ac} = 100$  Hz.

(Fig. 5 (a) and (c)); in the other hand, the displacement of the recirculation center visible in the velocity map in the case  $G/H = 0.04$  is much less marked (Fig. 5 (b) and (d)). Moreover, in the low actuation frequency case, the velocity fluctuations (not shown here for conciseness) are comparable in magnitude to that presented in Fig. 4 of [5]. In a large part of the wake-flow, the high velocity fluctuations are a consequence of a highly non-stationary process; this process is therefore analyzed in the following by use of a triple decomposition.

3.2.3. Phase averaging for controlled cases

In Fig. 6 are presented the phase average of  $y$ -component vorticity,  $\langle \omega_y \rangle(\mathbf{x}, \tau)$ , as defined in Eq. (3) for different time delay  $\tau$  covering a complete actuation cycle and for the two actuation frequencies studied in the previous section. For the control at frequency  $F_{ac} = 10$  Hz (Fig. 6.1), two perturbations are induced successively in the wake-flow. One, generated when the control jets start (a), develops in the shear layer with a convection speed about  $U_\infty/2$ . This structure is thus visible in (b) around  $X/H = 1.5$ , and keeps on being convected such that it leaves the field of view in the following map. After, the phase average vorticity is mainly associated with a nearly-constant shear within the shear layer (c to e). The other



**Fig. 6.** (Color online.) Maps of  $\langle \omega_y \rangle$  for the  $G/H = 0.04$  configuration with control at  $F_{ac} = 10$  Hz (I) and 100 Hz (II). The maps are equally spaced within one actuation cycle, which corresponds to a difference in time delay  $\tau$  between two successive maps of  $1/9/F_{ac}$ ; the map (a) corresponds to the beginning of blowing. For color coding, see online the color map of Fig. 7.

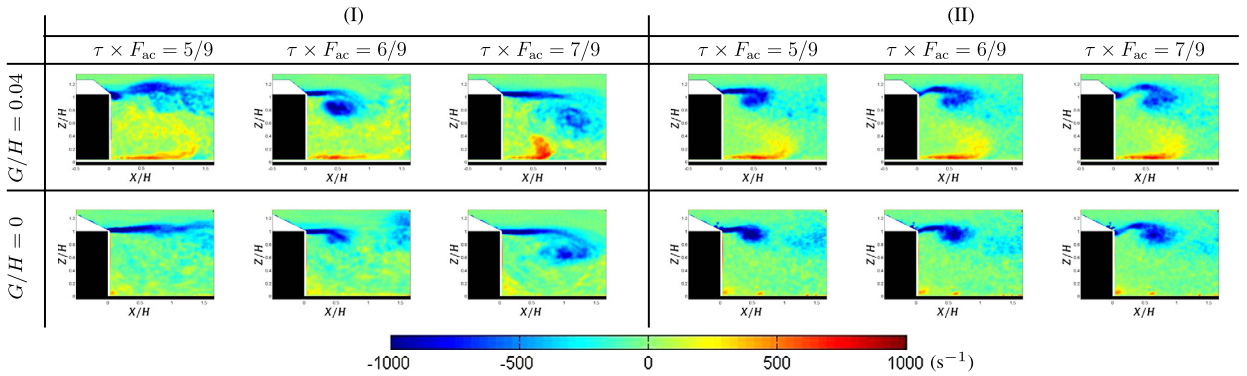


**Fig. 7.** (Color online.) Maps of  $\langle \omega_y \rangle$  with control at  $F_{ac} = 10$  Hz (I) and 100 Hz (II). The results obtained for the configurations  $G/H = 0$  and 0.04 are compared at values of  $\tau \times F_{ac}$  of 5/9, 6/9 and 7/9.

perturbation is associated with the stop in control jets blowing (f). This structure rolls-up in such a way that it interacts with the underbody flow and develops over a vertical dimension close to the model height (g and h). It may be assumed that such perturbations (or at least one of these perturbations) are responsible for a decrease in the mean pressure coefficient, because they may impose periodically an overall drop in the base pressure. These two perturbations apparently do not interact before  $X/H = 1.6$ , because their convection speed and the time delay of  $1/2/F_{ac}$  corresponding to the duty-cycle of 50% imposed to the control jets are sufficiently high. Thus, it is obvious that for actuation frequencies lower than 10 Hz, these two structures during each actuation cycle will not interact close to the model base. As a consequence, the same kind of structures induced directly (at the beginning of blowing) or indirectly (at the end of blowing) is to be found for any actuation frequency at least up to 10 Hz. For an actuation frequency of 5 Hz for instance, these two perturbations will occur two times less than for an actuation frequency of 10 Hz, but with the same magnitude. This may explain the good fit between the experimental data and the linear behavior of the left part of the curves in Fig. 2, between  $F_{ac} = 0$  and 10 Hz. As long as no interaction occurs, the linear behavior of  $C_p^{ref}$  with  $F_{ac}$  prevails. The analysis now concerns the data in Fig. 6.II where  $F_{ac} = 100$  Hz. When the control jets start (a), a small perturbation is induced next to the top base, in the vicinity of an existing structure coming from the previous actuation cycle, as highlighted hereafter. These two structures interact (b) and the resulting pattern develops as it is convected downstream (c to f). After the stop of control jets (f), one perturbation is induced in the flow, into the form of an undulation of the shear layer (g), which partly interacts with the existing structure (g). In the same time, part of the undulation of the shear layer rolls-up around the model base, and forms the vortical structure that will interact at the beginning of the next actuation cycle with the new perturbation introduced. Thus this interaction promote a mechanism that differs from that observed at  $F_{ac} = 10$  Hz.

Phase average results for the two values of ground clearance are given for  $F_{ac} = 10$  Hz and 100 Hz in Fig. 7. For the highest actuation frequency (Fig. 7.II), one may note that the phase average vorticity maps present the same features in the two configurations. For example, the undulation of the shear layer associated with the stop of control jets is very well

retrieved in the  $G/H = 0$  case. This is interpreted as the result of the little influence, for this actuation frequency, of the underbody flow on the development of the structures in the upper shear layer. Indeed, a closer observation of Fig. 6.11 indicates that the characteristics of the phase average vorticity in the underbody flow region are quite constant from one time delay  $\tau$  to another, which holds also in the configuration related to Fig. 7.11 and suggests that the underbody flow does not present a significant response at the actuation frequency. The same comparison for  $F_{ac} = 10$  Hz (Fig. 7.1) indicates that, to some extent, the similarity between the two configurations also holds. One may notice that the vortical patches in the maps obtained for  $\tau F_{ac} = 6/9$  are a bit different in intensity and location, and that those visible in the maps obtained for  $\tau F_{ac} = 7/9$  also differs in orientation. This is postulated to result from the interaction with the underbody flow in the  $G/H = 0.04$  case. These results are finally used to determine possible links between the vortical structures induced by the control and the local diminution of pressure over the model base. In the  $F_{ac} = 10$  Hz case, in both configurations, two noticeable vortices were induced in the flow in phase opposition by the control, and convected downstream. From a phase average point of view, it exists in this case phases during an actuation cycle where the wake-flow do not present vortical structures close to the model, but is essentially marked by mean shear in the shear layer. In the  $F_{ac} = 100$  Hz case, again for both configurations, the interaction between the generated structures happen close to the model. These structures remain smaller than that observed for  $F_{ac} = 10$  Hz, but they are present in the wake-flow for all the phases examined in the phase average study. Thus, the very similar values of  $\overline{C_p}$  obtained for these two actuation frequencies are likely to result from a balance between the intensity of the vortical structures generated by the control and the frequency at which they are generated.

#### 4. Conclusions

This experimental study of flow control around a square back model focuses on the influence of an underbody flow between the model and the floor on the control effects. The phase average analysis indicate that the perturbations induced by the control dominate over the natural wake-flow differences between the configurations with or without underbody flow. Striking similarities between controlled cases particularly for the high actuation frequency cases are observed. The role of the actuation frequency is also considered, by comparing pressure coefficient data and wake-flow characteristics for two actuation frequencies, chosen because they offer highly comparable values in  $\overline{C_p}$  reduction. The study of the vortical structures development in each case suggests that a balance between the intensity of the vortical structures generated by the control and the frequency at which they are generated governs the  $\overline{C_p}$  reduction. Further developments of the present analysis will rely on synchronized pressure–velocity measurements in the wake flow to correlate the evolution of the pressure on the model base over one actuation cycle and the generation and development of vortical structures in the main shear layer.

#### References

- [1] K.B. Chun, H.J. Sung, Control of turbulent separated flow over a backward-facing step by local forcing, *Exp. Fluids* 21 (6) (1996) 417–426.
- [2] G. Bosch, M. Kappler, W. Rodi, Experiments on the flow past a square cylinder placed near a wall, *Exp. Therm. Fluid Sci.* 13 (3) (1996) 292–305.
- [3] L.L. Shi, Y.Z. Liu, H.J. Sung, On the wake with and without vortex shedding suppression behind a two-dimensional square cylinder in proximity to a plane wall, *J. Wind Eng. Ind. Aerodyn.* 98 (10–11) (2010) 492–503.
- [4] H. Choi, W.-P. Jeon, J. Kim, Control of flow over a bluff body, *Annu. Rev. Fluid Mech.* 40 (1) (2008) 113–139.
- [5] S. Chaligné, T. Castelain, M. Michard, D. Juvé, Active control of the flow behind a two-dimensional bluff body in ground proximity, *C. R. Mécanique* 341 (2013) 289–297.
- [6] K.P. Garry, Some effects of ground clearance and ground plane boundary layer thickness on the mean base pressure of a bluff vehicle type body, *J. Wind Eng. Ind. Aerodyn.* 62 (1) (1996) 1–10.
- [7] S. Chaligné, T. Castelain, M. Michard, E. Jondeau, D. Juvé, Contrôle d'écoulement autour d'un corps non profilé bidimensionnel en interaction avec le sol, in: 21<sup>e</sup> Congrès français de mécanique, Bordeaux, France, 2013.